scientific reports

OPEN

Synthesis and characterization of Se doped Fe$_3$O$_4$ nanoparticles for catalytic and biological properties

Mohammad Reza Ahghari, Zeinab Amiri-khamakani & Ali Maleki✉

In this study, Se-doped Fe$_3$O$_4$ with antibacterial properties was synthesized using by a coprecipitation method. The chemistry and morphology of the Se doped Fe$_3$O$_4$ nanocomposite were characterized by energy-dispersive X-ray spectroscopy, field-emission scanning electron microscopy, X-ray diffraction, vibrating sample magnetometry, and Brunauer–Emmett–Teller spectroscopy. The antibacterial activity of the Fe$_3$O$_4$/Se nanocomposite was examined against G$^+$ (Gram-positive) and G$^-$ (Gram-negative) bacteria, in the order *Staphylococcus aureus*, *Staphylococcus saprophyticus*, *Pseudomonas aeruginosa*, *Klebsiella pneumonia*, and *Escherichia coli*, which are the most harmful and dangerous bacteria. Fe$_3$O$_4$/Se, as a heterogeneous catalyst, was successfully applied to the synthesis of pyrazolopyridine and its derivatives via a one-pot four-component reaction of ethyl acetoacetate, hydrazine hydrate, ammonium acetate, and various aromatic aldehydes. Fe$_3$O$_4$/Se was easily separated from the bacteria-containing solution using a magnet. Its admissible magnetic properties, crystalline structure, antibacterial activity, mild reaction conditions, and green synthesis are specific features that have led to the recommendation of the use of Fe$_3$O$_4$/Se in the water treatment field and medical applications. Direct Se doping of Fe$_3$O$_4$ was successfully realized without additional complicated procedures.

In recent years, nanotechnology has been hailed as a ground-breaking field that ushered in a new era in applied sciences and technology[1,2]. Synthesized nanomaterials have many broad applications in a variety of fields, including pharmaceutical, medical, cosmetic, and electrical applications. Of course, the materials are classified as nanoscale with at least one dimension of less than 100 nm. These materials were considered when researchers discovered that the size had a significant impact on the physical and chemical properties of the material[3,4]. Nanomaterials have a lot of fantastic and unique properties including that some of these materials have the potential ability to eliminate bacterial infections. Since today in the world because of excessive antibiotics, the growth of infectious bacteria resistant to these drugs is increasing day by day, the ineffective of these drugs against infectious bacteria is a serious threat to the world. However, some nano-sized compounds have appeared against such very strong bacteria, which has led to the attention of the global scope to nanomaterials[5–10]. One of the compounds that has long been known to humans is magnetite, Fe$_3$O$_4$, which is a common magnetic iron oxide with an inverted cubic spinel structure created by oxygen-iron bonding, where Fe (III) ions occupy both tetrahedral and octahedral sites. Fe$_3$O$_4$ nanoparticles are one of the most widely used magnetic compounds owing to their various applications and remarkable properties[11–14]. Functionalization of the surface of iron oxide nanoparticles with biocompatible materials increases the properties of this material, including colloidal stability and reduction of cytotoxicity[15,16]. Selenium is one of the most essential trace elements, in the human body and is an enzymatic antioxidant[17–19]; particularly vulnerable patients suffer from phenylketonuria, so individuals with diet-related diseases experience severe selenium deficiency. Additionally, individuals exposed to specialized chemotherapy and those who have already undergone radiotherapy are vulnerable to a decrease the amount of this element in vulnerable organisms. Selenium has biological activities, including antibacterial, anti-inflammatory, antiviral, antiparasitic, antifungal, and anticancer activities[20–22]. In addition this element is nanosized, due to its proper interaction with functional groups (C–O, C–N., NH, and COO–) of proteins that possess good adsorptive and biological activity[23–26]. The application of selenium nanoparticles in the field of biomedicine because of their unique properties, such as nutritional properties, environmental friendliness, and good chemotherapy, is very

Catalysts and Organic Synthesis Research Laboratory, Department of Chemistry, Iran University of Science and Technology, Tehran 16846-13114, Iran. ✉email: maleki@iust.ac.ir

noticeable[27–29]. Selenium, because of its antioxidant properties, increases cellular defense against oxidative stress in the cells of living organisms, including humans[30–33]. The mechanism of action of selenium is as follows: selenium functions as a redox center[24,34]; the best-known example of this redox function is the reduction of hydrogen peroxide and damaging lipid and phospholipid hydroperoxides to harmless products (water and alcohols) via the family of selenium-dependent glutathione peroxidases[2,24,35,36]. This function helps maintain membrane integrity, protects prostacyclin production, and reduces the likelihood of propagation of further oxidative damage to biomolecules such as lipids, lipoproteins, and DNA with the associated increased risk of bacterial infections, atherosclerosis, and cancer[23,36]. Drinking water is one of the most important and consumed substances by living organisms, and the life of most living organisms depends on water[37–40]. Drinking water is a suitable environment for growing bacteria, due to various factors such as inadequate disinfection[41–43], the proper temperature, and the presence of nutrients, which causes water pollution and is a danger to human health[44–46]. Some hazardous bacteria found in water include G+ *Staphylococcus saprophyticus*, *Staphylococcus aureus*, and G− *E. coli,* bacteria. In addition to water contamination, these bacteria are among the main causes of food poisoning[47–51]. Common Gram-negative bacteria. *Pseudomonas aeruginosa* is an opportunistic infection that is a major cause of illness and death in patients with cystic fibrosis and immunocompromised patients. The eradication of *P. aeruginosa* has become increasingly challenging because of its extraordinary ability to withstand medicines[52,53].

Pseudomonas aeruginosa strains have a high degree of innate and acquired resistance mechanisms, which they use to evade most drugs[54].

Furthermore, among Gram-negative bacteria, *Klebsiella pneumonia* is the predominant ESBL producer associated with urinary tract infection, and sometimes it progresses to more important infections, such as blood poisoning[55,56].

Therefore, the G− *E. coli* bacterium is the most common cause of urinary tract infections[57], and the G+ *S. aureus* bacterium that causes skin infections such as abscesses, respiratory infections, including sinusitis, and food poisoning. Infections are frequently facilitated by pathogenic strains that release virulence factors, such as strong protein toxins, and produce a cell surface protein that binds and inactivates antibodies[58]. However, owing to their strong antibacterial properties, selenium-containing compounds can help remove bacteria from water. Selenium-containing compounds play an important role in organic synthesis, biochemistry, medicinal chemistry, and materials science. They can be used as nucleophiles, electrophiles, ligands, and catalysts in organic syntheses[59]. Selenium-catalyzed reactions have attracted extensive attention because of the advantages of mild and eco-friendly reaction conditions, good functional compatibility, excellent selectivity, high atom economy, and low cost. In the synthesis of biologically active organic compounds, multicomponent reactions (MCRs) with attributes such as experimental simplicity, synthetic efficiency, and formation of several bonds in one unit operation have been suggested, particularly in the case of heterocyclic compounds, such as pyrazolopyridine derivatives which are an essential system because of their confirmed utility as organic fluorophores, bioactive compounds, and ligands to coordination complexes[14,60,61]. These derivatives are an important class of nitrogen-containing heterocyclic chemicals with antileishmanial, antibacterial, and antiviral properties. Because the pyrazolopyridine nucleus is structurally similar to purines, its derivatives may compete with purines and prevent nucleic acid production. Several pyrazolopyridines have been to interact with DNA and limit the proliferation of cancer cell types[62–65]. By combining materials with potential properties, new materials with better and more effective performance can be created. In this study, the surfaces of Fe_3O_4 nanoparticles were coated with selenium nanoparticles, as a result of the performance of the new material synthesized as a nanocomposite in two different departments. The removal of bacterial contaminants from drinking water can also, be easily isolated from solutions containing bacteria using a magnet. The nanocomposite effectively killed pathogenic human bacteria. Additionally, it is a powerful catalyst for the synthesis of organic compounds with drug properties.

Experimental

General. Chemical materials were produced from Sigma–Aldrich, and Merck were purchased and used without additional purification. The following is a list of analytical device information: The TESCAN4992 instrument was used to record the energy-dispersive X-ray (EDX) analyses. Using a TESCAN4992, powder X-ray diffraction (XRD) patterns of the nanocomposites. The specific surface area and degree of porosity of the prepared samples were determined using the Brunauer–Emmett–Teller adsorption–desorption isotherm (BET., Micrometics ASAP2020). A Sigma-Zeiss microscope was used to capture pictures of the nanocomposite using field emission scanning electron micrographs (FESEM). An accurate magnetometer (Iran Kavir VSMs) was used to measure the magnetic properties of the solid object. The melting points were calculated using an electrothermal 9100 device. ¹H and ¹³C nuclear magnetic resonance (NMR) spectra were recorded on a Bruker DRX-300 Avance spectrometer at 300 MHz and 75 MHz, respectively. The antibacterial activity of the nanocomposite against the pathogenic bacteria *Staphylococcus aureus* (*S. aureus*) (ATCC 12,600), *Staphylococcus saprophyticus* (*S. saprophyticus*) (ATCC 1440), G− *Escherichia coli* (*E. coli*) (ATCC 9637*)*, *Klebsiella pneumonia* (*K. pneumonia*) (ATCC 700,603), and *Pseudomonas aeruginosa* (*P. aeruginosa*) (ATCC 27,853) was studied.

Syntheses of Fe_3O_4/Se. First, using the sedimentation method, distilled water (200 mL) was used to dissolve the co-deposition of $FeCl_3 \cdot 6H_2O$ (20 mmol) and $FeCl_2 \cdot 4H_2O$ (20 mmol) salts, and the mixture was stirred at room temperature for approximately 50 min under a N_2 atmosphere. The temperature was gradually increased to 85 °C. Subsequently, 10 mL of ammonium hydroxide (25%) was added dropwise to the stirring solution to provide iron oxide NPs at pH = 12. Finally, the Fe_3O_4 Nps magnetic dark precipitate was collected by an external magnetic field and washed with deionized water three times. In the continuous synthesis step, Fe_3O_4 NPs were dispersed in 10 ml of ethanol under intense stirring, and then, 1 g of selenium dioxide was added to the mixture and stirred at room temperature for 30 min. Sodium borohydride (0.03 g) was added and the mixture was stirred

at room temperature. The prepared product was collected using an external magnetic field, washed with water and ethanol several times, and dried to afford a brown solid.

Common procedure for the synthesis of pyrazolopyridine derivatives 5a–j.

The catalytic activity of the Fe_3O_4/Se nanocomposite was tested in a one-pot synthesis of pyrazolopyridine derivatives. The four components were mixed and reacted in the presence of 1 ml EtOH at room temperature: hydrazine hydrate (2 mmol), ethyl acetoacetate (2 mmol), aromatic aldehydes (1 mmol), and ammonium acetate (3 mmol) (Table1). Thin-layer chromatography was used to evaluate reaction completion process (TLC). The undissolved magnetic nanocatalyst was separated from the reaction mixture using a magnet after completion of the reaction. To obtain pure pyrazolopyridine derivatives, the crude product was recrystallized from EtOH. All the products were well-known chemicals recognized by comparing their melting points with those in the original literature (Table 3).

Spectral data of selected products. Spectral data of selected products. Analysis of the results of NMR. 3, 5-Dimethyl-4-phenyl-1, 4, 7, 8-tetrahydrodipyrazolo [3, 4-b: 4′, 3′-e]Pyridine (5a): 1H NMR (300.13 MHz, DMSO-d6): δ = 2.06 (s,6H, CH3), 4.81 (s, 1H, CH), 7.14–7.20 (m, 5H, H-Ar), 11.24–11.32 (br s, 3H, NH); 13C NMR (75.47 MHz, DMSO-d6): δ = 10.8, 33.1, 104.6, 125.8, 127.9, 128.1, 140.2, 143.7, 161.5. IR (KBr: ū /cm − 1): 3528, 3301, 2925, 1614, 1515 and 1375.

4-(2,4-Dichloro-phenyl)-3, 5-Dimethyl-1, 4, 7, 8-tetrahydrodipyrazolo [3, 4-b: 4′, 3′-e]pyridine(5b):1H NMR (300.13 MHz, DMSOd6): δ = 1.95 (s, 6H, CH3), 5.06 (s, 1H, CH), 7.33 (dd, J1 = 2.1 Hz,J2 = 8.4 Hz, 1H, H-Ar), 7.47 (d, J = 2.1 Hz, 1H, H-Ar), 7.49 (d ,J = 8.4 Hz, 1H, H-Ar), 11.08 (br s, 3H, NH); 13C NMR(75.47 MHz, DMSO-d6): δ = 15.62, 36.37, 107.01, 131.71,133.56, 136.19, 137.10, 138.41, 143.80, 145.18,165.75.

4-(2-nitro-phenyl)- 3, 5-dimethyl-1, 4, 7, 8-tetrahydro-dipyrazolo [3, 4-b: 4′, 3′-e] pyridine(5c): 1H NMR (300.13 MHz, DMSO-d6): δ = 1.92 (s, 6H, CH3), 5.44 (s, 1H, CH), 7.37–7.68 (m, 4H, H-Ar), 10.98 (br s, 3H, NH); 13C NMR (75.47 MHz, DMSO-d6): δ = 10.0, 28.9, 101.9, 123.8, 127.1, 130.2,131.6, 136.2, 138.6, 149.5, 160.5.

4-(4-Bromo-phenyl)-3,5-dimethyl-1,4,7,8-tetrahydro-dipyrazolo[3,4-b;4′,3′-e]pyridine (5d): 1H NMR (300.13 MHz, DMSO-d6) δ = 2.07 (s,6H, CH3), 4.78 (s, 1H, CH), 7.04 (d, J = 8.3 Hz, 2H, H-Ar), 7.37 (d, J = 8.4 Hz, 2H, H-Ar), 11.32 (br, s, 3H, NH); 13C NMR (75.47 MHz, DMSO-d6): δ = 10.2,32.2, 104.4, 118.4, 129.7, 130.4, 131.9, 142.7, 157.5.

4-(4-Chlorophenyl)-3,5-dimethyl-1,4,7,8-tetrahydrodipyrazolo[3,4-b:4′,3′-e]pyridine (5e):1H NMR (300.13 MHz, DMSO-d6): δ = 2.06 (s, 6H, CH3), 4.80 (s, 1H, CH),7.12 (d, J = 7.1 Hz, 2H, H-Ar), 7.24 (d, J = 7.2 Hz, 2H, H-Ar), 11.35 (br s, 3H, NH); 13C NMR (75.47 MHz, DMSO-d6): δ = 10.7,32.6, 104.3, 128.0, 129.8, 130.4, 140.1, 142.7, 161.4. IR (KBr, ū/cm − 1): 3365, 3100, 2854, 1612, 1526, and 1368.

4-(4-methyl-phenyl)- 3, 5-dimethyl-1, 4, 7, 8-tetrahydro-dipyrazolo [3,4-b:4′,3′-e] pyridine (5f.): 1H NMR (300.13 MHz, DMSO-d6): δ = 2.04 (s, 6H, CH3), 2.21 (s, 3H, CH3), 4.74 (s, 1H, CH), 6.98–7.00 (m, 4 H, H-Ar), 11.24 (s,3H, NH);13C NMR (75.47 MHz, DMSO-d6): δ = 10.8, 20.9, 32.8, 104.8, 127.8, 128.8, 134.7, 140.2,140.7, 161.5.

4-(4-nitro-phenyl)-3,5-Dimethyl-1,4,7,8-tetrahydro-dipyrazolo[3,4-b:4′,3′-e]pyridine(5 g):1H NMR (300.13 MHz,DMSO-d6): δ = 2.07 (s, 6H, CH3), 4.95 (s, 1H, CH), 7.34–7.36 (d, 2 H, J = 8 Hz,2H, H-Ar), 8.09–8.11 (d, 2 H, J = 8 Hz, 2H, H-Ar), 11.25 (s, 3H, 3 NH); 13CNMR (75.47 MHz, DMSO-d6): δ = 10.75, 33.43, 103.62, 123.46, 129.25, 140.18,146.09, 152.24, 161.34.

4-(3,5-Dimethyl-1,4,7,8-tetrahydro-dipyrazolo[3,4-b;4′,3′-e]pyridin-4-yl)-phenyl]-dimethylamine(5 h): 1H NMR (300.13 MHz, DMSO-d6) δ = 2.05 (s, 6H, CH3), 2.8 (s, 6H, CH3), 4.69 (s,1H, CH), 6.56(d, J = 8.8 Hz,2H, H-Ar), 6.92 (d, J = 8.5 Hz, 2H, H-Ar), 10.91 (br, s,3H, NH); 13C NMR (75.47 MHz, DMSO-d6):δ = 10.3, 31.7, 40.4, 104.7, 112.2, 127.8, 131.1, 148.5, 159.7, 161.0.

4-(4-Cyano-phenyl)-3, 5-Dimethyl-1, 4, 7, 8-tetrahydrodipyrazolo [3,4-b;4′,3′-e]pyridine(5i):1H NMR (300.13 MHz,DMSO-d6): δ = 2.09 (s, 6H, CH3), 4.93 (s, 1H, CH), 7.32 (d,J = 8.1 Hz, 2H, H-Ar), 7.70 (d, J = 8.1 Hz, 2H, H-Ar), 11.39 (br s,3H, NH); 13C NMR (75.47 MHz, DMSO-d6): δ = 10.77, 33.49, 103.76, 108.72, 119.61, 129.08, 132.19, 140.26,149.91, 161.36.

4-(4-Fluoro-phenyl)-3, 5-Dimethyl-1, 4, 7, 8-tetrahydrodipyrazolo [3,4-b;4′,3′e]pyridine(5j):1HNMR(300.13 MHz,DMSOd6): δ = 2.08 (s, 6H, CH3), 4.83 (s, 1H, CH), 7.03 (t, J = 8.9 Hz, 2H, H-Ar),7.15 (dd, J1 = 5.9 Hz, J2 = 8.4 Hz, 2H, H-Ar), 11.35 (br s, 3H, NH)ppm; 13C NMR (75.47 MHz, DMSO-d6): δ = 10.79, 32.57,104.61, 114.74 (J = 21 Hz), 129.67 (J = 7.9 Hz), 139.81(J = 2.8 Hz), 140.10, 160.88 (J = 240 Hz), 161.44.

4-(4-hydroxy-phenyl)-3, 5-Dimethyl-1, 4, 7, 8-tetrahydrodipyrazolo [3,4-b;4′,3′-e]pyridine(5 k):1H NMR (300.13 MHz, DMSO-d6): δ = 2.03 (s, 6H, CH3), 4.65 (s, 1H, CH), 6.56–6.58 (d, J = 8 Hz, 2 H, H-Ar),6.88–6.90 (d, J = 8 Hz, 2H, H-Ar), 9.10 (s, OH), 11.50 (s, 3H, NH); 13CNMR (75.47 MHz, DMSO-d6): δ = 10.32, 31.75, 104.5, 114.42, 128.23, 133.35, 139.76,155.03, 161.04.

4-(4-Methoxy-phenyl)-3, 5-dimethyl-1, 4, 7, 8-tetrahydro-dipyrazolo [3,4-b;4′,3′-e] pyridine (5 l): 1H NMR (300.13 MHz, DMSO-d6): δ = 2.03 (s, 6H, CH3), 3.82 (s ,3H, CH3), 4.53 (s, 1H, CH),7.03 (d, J = 8.7 Hz, 2H,

Sample	Surface area[a] (m²/g)	Pore volume[b] (cm³/g)	Pore size[b] (nm)
Selenium-coated Fe_3O_4	11.57	0.073406	6.95

Table 1. Surface area, pore volume, and pore diameter of the Fe_3O_4/Se nanocomposite. [a]The surface area was obtained by BET analysis. [b]Pore volume and pore diameter obtained by BJH analysis.

H-Ar), 7.79 (d, J = 8.6 Hz, 2H, H-Ar), 8.99 (br, s, 3H, NH); 13C NMR (75.47 MHz, DMSO-d6): δ = 10.3, 31.9, 54.9, 104.4, 113.0, 128.3, 135.1, 139.6, 157.1, 161.0.

The FT-IR spectrum results are characterized in the supplementary information (Figs. S1, S6). Antibacterial test. The antibacterial activity of Fe_3O_4@Se was tested against five bacterial strains using agar diffusion and colony counting methods. The cultivation perimeter was prepared by dissolving a certain amount of powdered Muller–Hinton agar in distilled water. The Prepared dissolved culture medium and all instruments were sterilized for approximately 15 min at 121 °C and pH = 7.3 in an autoclave.

Evaluation of agar diffusion. In disk diffusion tests, the suspensions with 0.5 McFarland turbidity of *S. aureus*, *S. saprophyticus, P. aeruginosa, E. coli,* and *K. pneumonia,* strains have been prepared. Then, 10 mg of Fe_3O_4@Se nanocomposite powder was added to the Muller-Hinton agar plate containing bacteria, and the sample-loaded disks for the plates were incubated at 37 °C for 24 h. The ability of the Fe_3O_4@Se nanocomposite to effectively inactivate bacteria was much greater than that of the other studied samples, including, the bare Fe_3O_4 nanoparticles (Figs. 6, S8)[48].

Plate-count method. One of the most important and practical methods for determining the concentration of microbes in a sample is to dilute the sample, grow the microbes on the plates and count the colonies.

Staphylococcus aureus and *E. coli* colonies after cultivation for 24 h on Fe_3O_4@Se and control samples were compared. As shown in Fig. 7,[48] the number of bacterial colonies was considerably reduced by treatment with the Fe_3O_4@Se nanocomposite in comparison with the control samples of *S. aureus* and *E. coli.*

Results and discussion

EDX analysis. EDX was used for the initial analysis of the Fe_3O_4/Se nanocomposites. The presence of high-intensity peaks related to O, Fe, and Se indicates nanocomposite components. This is shown in (Fig. 1)[49]. According to the weight percentage table of the components of the Fe_3O_4/Se nanocomposite, the most abundant element in this nanocomposite was Fe, which had the highest weight percentage (37.25%), followed by oxygen (32.93%), which had the highest weight ratio, and selenium (29.82), which had the appropriate weight percentage.

XRD analysis. The X-ray diffraction (XRD) pattern of the produced Fe_3O_4/Se nanocomposite was examined to verify the impact of the composited components on the overall crystal structure (Fig. 2). The diffraction peaks at 2θ = 18.36, 30.2, 35.5, 43.1, 57.1, 62.7, and 74.3 corresponded to the (111), (220), (3 1 1), (400), (4 2 2), (511), (4 4 0), and (533) diffraction planes of magnetite Fe_3O_4 NPs with a crystal structure that is in excellent agreement with the reported JCPDS 01-088-0315[37]. Three prominent diffraction peaks at 2θ = 30.141°, 56.999°, and 62.667° are related to the (1 0 1), (1 1 2), and (022) diffraction planes of Se with a crystal hexagonal structure, which is in reasonable agreement with the reported JCPDS card no 01-086-2244. The XRD results for the Fe_3O_4/Se NPs indicated that the crystal arrangement of the Fe_3O_4 core did not change throughout the functionalization route. Based on this information, the average crystallite size of the Fe_3O_4/Se NPs was approximately 20 nm. The crystallite size was calculated by the Debye–Scherrer aquation using Eq. (1), as follows:

$$D_P = 0.94\lambda/\beta \cos\theta \qquad (1)$$

Since the catalyst has been used several times in the reaction in this regard, the primitive pattern of this nanocomposite was compared with the secondary separate pattern of the Fe_3O_4/Se nanocomposite after six cycles of use in the organic reaction pyrazolopyridine, as seen in (Fig. S7), XRD analysis of the consumed catalyst underwent changes after six cycles of use, but there are still index peaks related to the crystal structure of the nanocomposite, which confirms the preservation of the catalyst structure. However, new peaks also appeared, which could be due to impurities in the products or reactants on the surface of the recycled catalyst. (See Supplementary Information).

FESEM and TEM analysis. Used to observe particle size distribution, surface morphology, and particle aggregation mode in prepared samples Field-emission scanning-electron microscopy (FESEM) and transmission electron microscopy (TEM) analyses were utilized to examine morphologies and structure. As shown in Fig. 3[4], the FESEM images of the Fe_3O_4/Se NPs are presented at three scales: 1 μm, 500 nm, and 200 nm. The Fe_3O_4/Se images showed a spherical structure, in the nanocomposite images, in addition to the spherical structure, the distribution of Se NPs on the Fe_3O_4 support was also observed. The average particle size of the 35 spherical particles in the nanocomposite was determined to be approximately 80 nm in addition, As is seen in the TEM image, the spots distributed around the magnetic nanoparticles represent the Se, which confirms the good composition of the Se with the Fe_3O_4 also Se acts as the matrix of the inorganic composite.

The N_2 adsorption–desorption isotherm. The N_2 adsorption–desorption isotherm of Fe_3O_4/Se is shown in Fig. 4. Detailed information including the surface area, pore volume, and pore size (width) of the Fe_3O_4/Se catalytic system, calculated using the (Brunauer–Emmett–Teller (BET)) and (Barrett–Joyner–Halenda(BJH)) methods is presented in Table 1. The BET surface area and pore volume for Fe_3O_4/Se were recorded to be approximately 11.57 m²/g and 0.073 cm³/g, respectively, which are slightly less than reported values in the literature[66,67] for neat mesoporous Fe_3O_4 (15.63 m²/g and 0.25960 cm³/g). This observation can be mainly related to covering a certain number of Fe_3O_4 pores by embedding Se NPs onto the surface of the Fe_3O_4 pores, which resulted in less

| Element	Weight%
Fe	37.25
O	32.93
Se	29.82
Totals	100.00
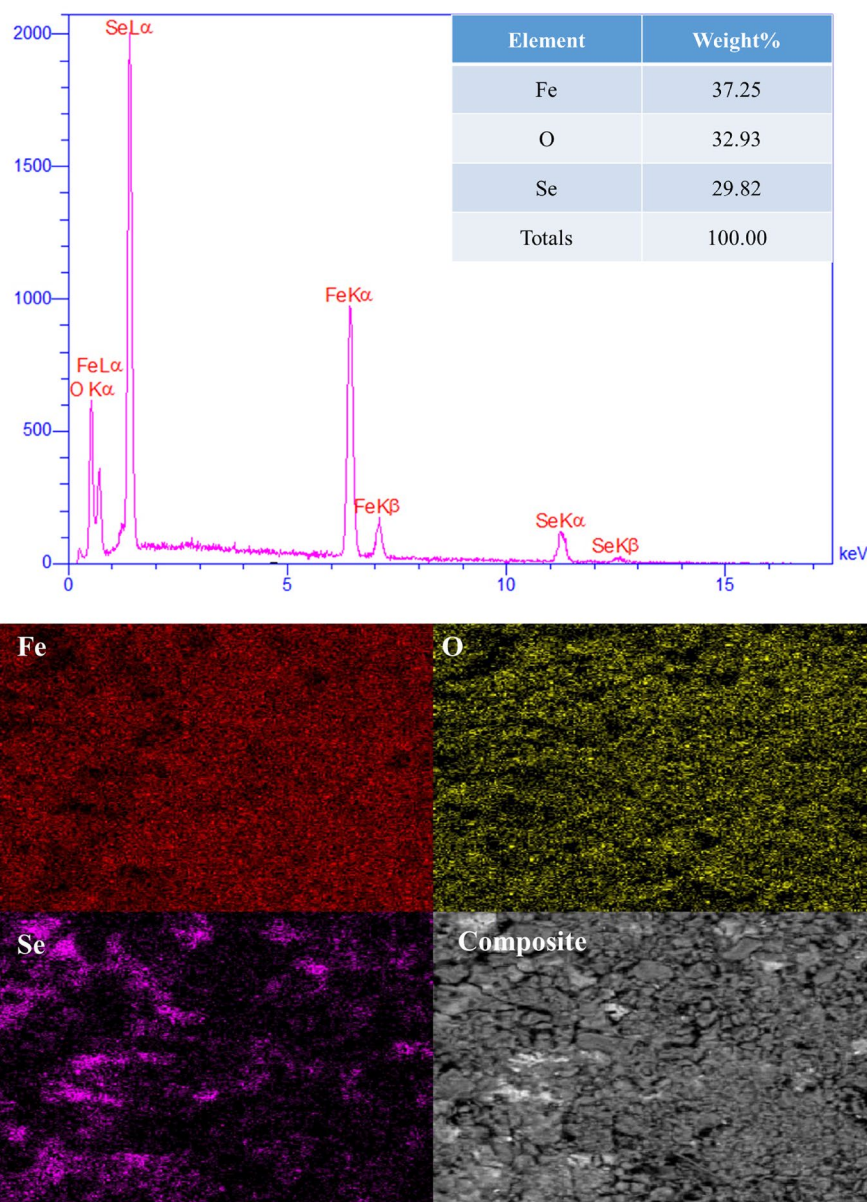
Figure 1. EDS spectra and elemental mapping images of Fe, Se, O, and the Fe_3O_4/Se NPs.

available surface area for gas adsorption and decreased pore volume. However, the Fe_3O_4/Se nanocomposite has a high surface area for promoting the catalytic reaction and antibacterial activity.

VSM analysis. VSM analysis was performed to determine the magnetic characteristics of the Fe_3O_4/Se hybrid catalyst. As shown in Fig. 5, The S-like magnetization curve showed no hysteresis loop, which indicates that both the remanence (Mr) and coercivity (Hc) were zero and confirmed the superparamagnetic nature of this hybrid catalyst. Magnetic measurements of ambient temperature from $-20,000$ to $+20,000$ showed that the saturation magnetization (Ms) value of the Fe_3O_4/Se nanocomposite compared to that of Fe_3O_4 was lowered to 20 emu g^{-1}, which was attributed to the addition of selenium to the catalyst reducing the mass percentage of magnetic Fe_3O_4/Se. Although Ms decreased, the hybrid catalyst still exhibited strong magnetic activity. And could be collected without difficulty from the reaction mixture using an external magnet (Figs. 6, 7).

Antibacterial activity. It was discovered that adding Se NPs to the mix might efficiently boost the generation of reactive oxygen species (ROS)[20]. The most widely accepted mechanism of accomplishment for Se NPs is particle attachment to the bacterial surface and the release of selenium ions into the bacterial cell, which results in oxidative stress, protein synthesis inhibition, or DNA mutation[68].

There are several putative mechanisms of action of Se NPs. Four possible modes of action were examined to determine whether they explain the antibacterial properties of Se NPs: (1) metabolic intrusion by disturbance
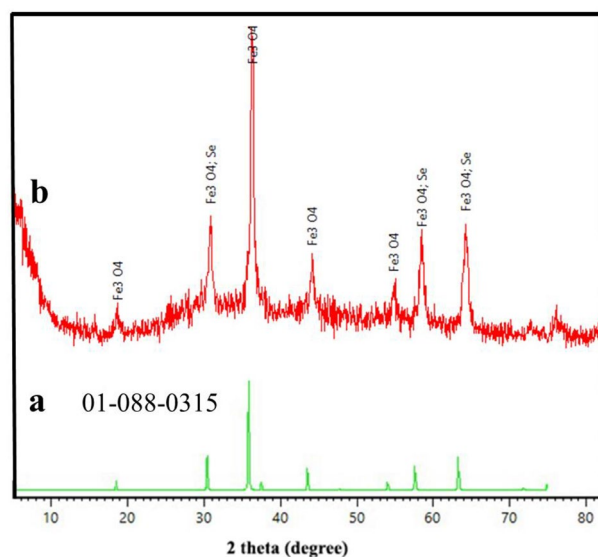
Figure 2. XRD pattern of (**a**) standard Fe_3O_4, and (**b**) the Fe_3O_4/Se.

of intercellular adenosine triphosphate (ATP) concentrations, (2) regulation of the intracellular concentration of reactive oxygen species (ROS), (3) bacterial membrane depolarization, and (4) bacterial membrane disruption. All living organisms use adenosine triphosphate (ATP) as an internal energy source. It is the most important energy source for many enzymatic processes; therefore, it is essential for respiration and metabolism. The energy-uncoupling effect is characterized by the rapid depletion of cellular ATP. Another mechanism that contributes to bacterial mortality is oxidative stress caused by excessive ROS production in response to nanoparticles[69].

Catalytic application. Another goal of Fe_3O_4/Se nanocatalyst production, as noted in the introduction, is to investigate its catalytic efficacy in organic processes.

In the synthesis of pyrazolopyridine derivatives, the catalytic activity of Fe_3O_4/Se was studied.

Different experimental conditions such as temperature, solvent, catalyst amount, and catalyst type were investigated in a one-pot four-component reaction of ethyl acetoacetate (2 mmol), hydrazine hydrate (2 mmol), 2, 4-dichlorobenzaldehyde (1 mmol), and ammonium acetate (3 mmol) as a model reaction to obtain the best result. First, the model reaction was carried out at two different temperatures without the use of a catalyst or solvent, and the yield of the products was 37% (Table 2, entry 3). The reaction yield was approximately 37% when the Fe_3O_4/Se nanocatalyst was added to the model in the absence of a solvent (Table 2, entry 3). Next, ethanol was added to the reaction in the presence of a catalyst at room temperature to analyze the solvent effect, and the efficiency increased significantly (Table 2, entry 4). The process was then repeated at 80 °C to determine how the temperature affected the outcome, and it was discovered that increasing the temperature to 80 °C caused the reaction to progress (Table 2, entry 5). Subsequently, under reflux and ultrasonic conditions, optimization studies were carried out in H_2O and EtOH as a green medium; the greatest efficiency was found in EtOH media at room temperature (Table 2, entries 6–8). Various concentrations of nanocatalyst were tested in addition to the reaction conditions and solvent, and the maximum yield of the product was reached in the presence of 0.03 g. (Table 2, entries 9 and 10). In the model reaction, the efficiency of the produced nanocomposite was compared to those of Fe_3O_4, Se, and Fe_3O_4/Se. The yield of a reaction in the presence of Fe_3O_4/Se is higher than Fe_3O_4 and Se separately, as indicated (Table 2, entries 12–13). Indeed, an Fe_3O_4/Se nanocatalyst with electrophilic selenium nanoparticles, a Lewis acid site (Fe^{3+} in Fe_3O_4), and a wide surface area worked as an efficient catalyst for the one-pot four-component reaction to produce pyrazolopyridine derivatives (Fig. 8).

Examination of the catalytic activity of Fe_3O_4/Se. The optimal conditions for synthesizing pyrazolopyridine derivatives using several types of aromatic aldehydes with hydrazine hydrate, ammonium acetate, and ethyl acetoacetate were investigated to assess the generality, application, and limitations between 35 and 90 min at room temperature. All aromatic aldehydes with electron-withdrawing and electron-donating substituents resulted in the synthesis of the corresponding high-yield products, as indicated in Table 3, with no byproducts detected.

Proposed mechanism. The most likely mechanism for the synthesis of different pyrazolopyridine derivatives with Fe_3O_4/Se nanoparticles is the four-step mechanism shown in Fig. 9. This is not only due to the abundant Lewis acid sites (Fe^{3+} of Fe_3O_4) and, to some extent, the high electrophilic properties of selenium nanoparticles, as well as their physical properties, large surface area, and high thermal and mechanical stability can play an important role in all steps of this four-step reaction illustrated in Fig. 9. Explaining the mechanism of this reaction according to the literature reports[62,70], first, due to the acidic sites of Fe and the electrophilic property of Se, the oxygen of the carbonyl ethyl acetoacetate groups is involved by the catalyst, which activates the car-
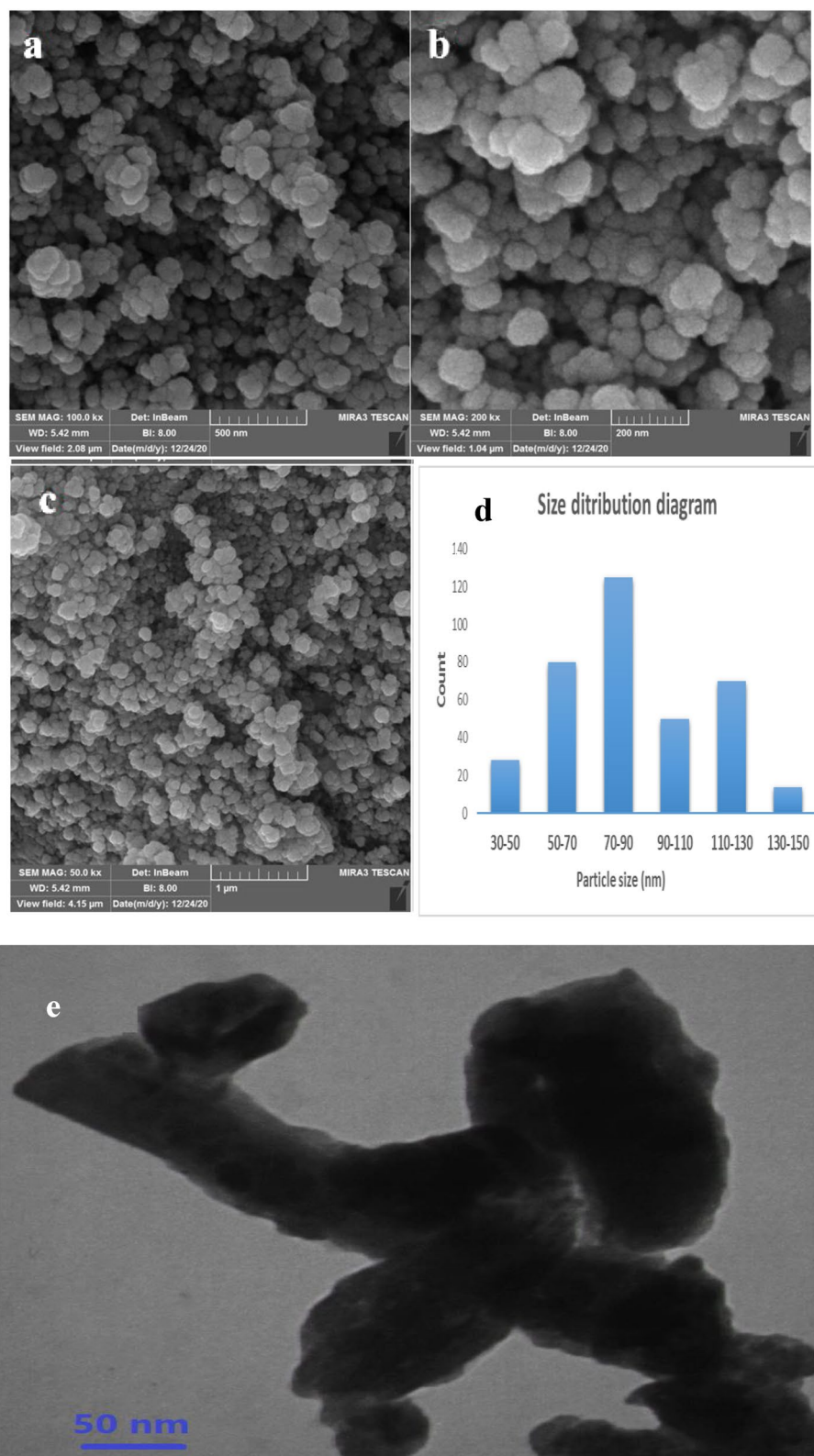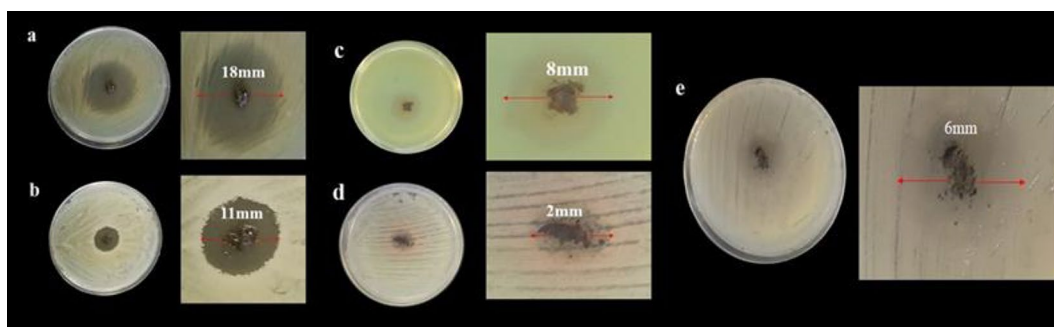
Figure 3. FESEM images of Fe_3O_4/SeNPs (**a**) 500 nm (**b**) 200 nm and (**c**) 1 μm and (**d**) particle size distributions (**e**) TEM images of Fe_3O_4/SeNPs.
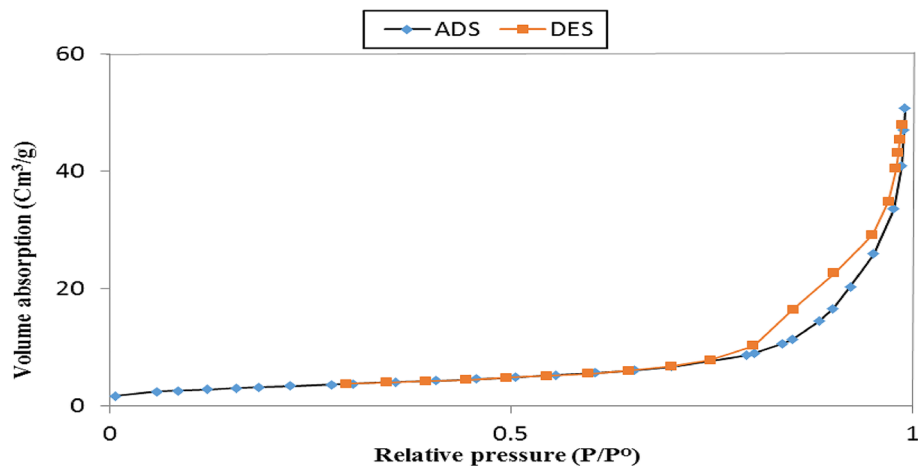
Figure 4. N$_2$ adsorption–desorption isotherms of Fe$_3$O$_4$/Se.

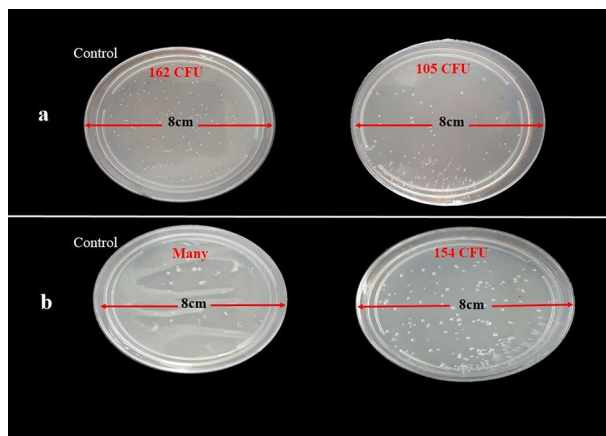| Sample	Ms (emu/g)	Mr (emu/g)	Hc (Oe)
Fe$_3$O$_4$	56	2	27
Fe$_3$O$_4$/Se	36	6	80
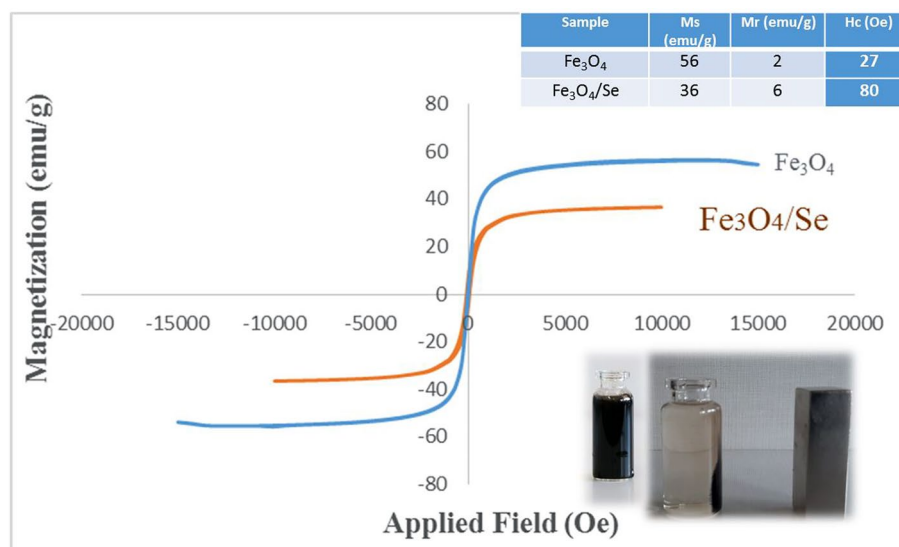
Figure 5. VSM magnetization curve of the Fe$_3$O$_4$/Se.

Figure 6. Agar disk diffusions of (**a**) *S. aureus*, (**b**) *E. coli*, (**c**) *P. aeruginosa*, (**d**) *S. saprophyticus*, and (**e**) *K. pneumonia* in the presence of Fe$_3$O$_4$/Se.

 8

Figure 7. Image colony formation unit (CFU) counting of (**a**) *S. aureus* and (**b**) *E. coli* in the absence and presence (on the right) of Fe_3O_4/Se.

Entry	Catalyst	Catalyst loading (g)	Solvent	Temp (°C)	Yield (%)[b]
1	_		_	r.t	Trace
2	_		_	80	Trace
3	Fe_3O_4/Se	0.02	_	r.t	37
4	Fe_3O_4/Se	0.02	EtOH	r.t	82
5	Fe_3O_4/Se	0.02	EtOH	80	87
6	Fe_3O_4/Se	0.02	H_2O	r.t	<41
7	Fe_3O_4/Se	0.02	H_2O	80	<50
8	Fe_3O_4/Se	0.02	EtOH	Ultrasonic, r.t	84
9	Fe_3O_4/Se	0.01	EtOH	80	76
10	Fe_3O_4/Se	0.03	EtOH	r.t	96
11	Fe_3O_4/Se	0.04	EtOH	r.t	98
12	Fe_3O_4	0.03	EtOH	r.t	37
13	Se	0.015	EtOH	r.t	35

**Table 2.** Optimizing the reaction conditions in the synthesis of pyrazolopyridine **5b**[a]. [a]Reaction conditions: ethyl acetoacetate (2 mmol), hydrazine hydrate (2 mmol), 3-nitrobezaldehyde (1 mmol) and ammonium acetate (1 mmol), catalyst (0.03 mg). [b]The yields relate to the isolated product.
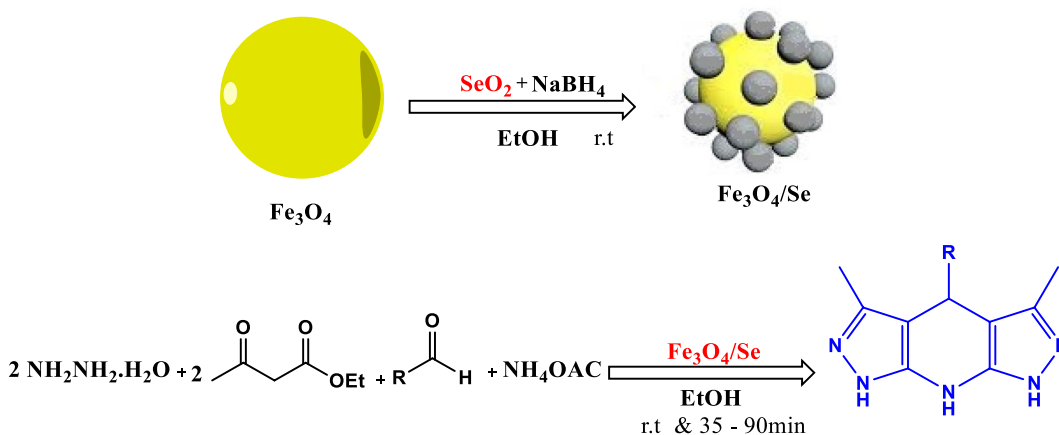
Figure 8. Synthesis of pyrazolopyridine (5a–l) derivatives using Fe_3O_4/Se. nanocomposites.

Entry	R	Product	Time (min)	Yield (%)	Mp	
					Found	Reported
1	C_6H_5	5a	60	91	241–243	240–242[70]
2	2,4-$(Cl)_2$–C_6H_3	5b	35	96	310	> 300[62]
3	2-NO_2–C_6H_4	5c	60	93	186–188	187–188[71,72]
4	4-Br–C_6H_4	5d	45	95	164–166	165–166[70,72]
5	4-Cl–C_6H_4	5e	60	96	254–256	255–257[73]
6	4-Me–C_6H_4	5f	75	92	245–247	244–246[74]
7	4-NO_2–C_6H_4	5g	60	93	297–299	295–297[62]
8	4-$(Me)_2N$–C_6H_4	5h	90	94	240–243	240–242[75]
9	4-CN–C_6H_4	5i	40	90	287–289	286–288[62]
10	4-F–C_6H_4	5j	90	89	258–260	259–261[62]
11	4-OH–C_6H_4	5k	40	97	267–269	269–271[76]
12	4-OMe–C_6H_4	5l	80	90	181–183	181–183[76]

Table 3. Synthesis of pyrazolopyridine derivatives 5a–l under optimal conditions.
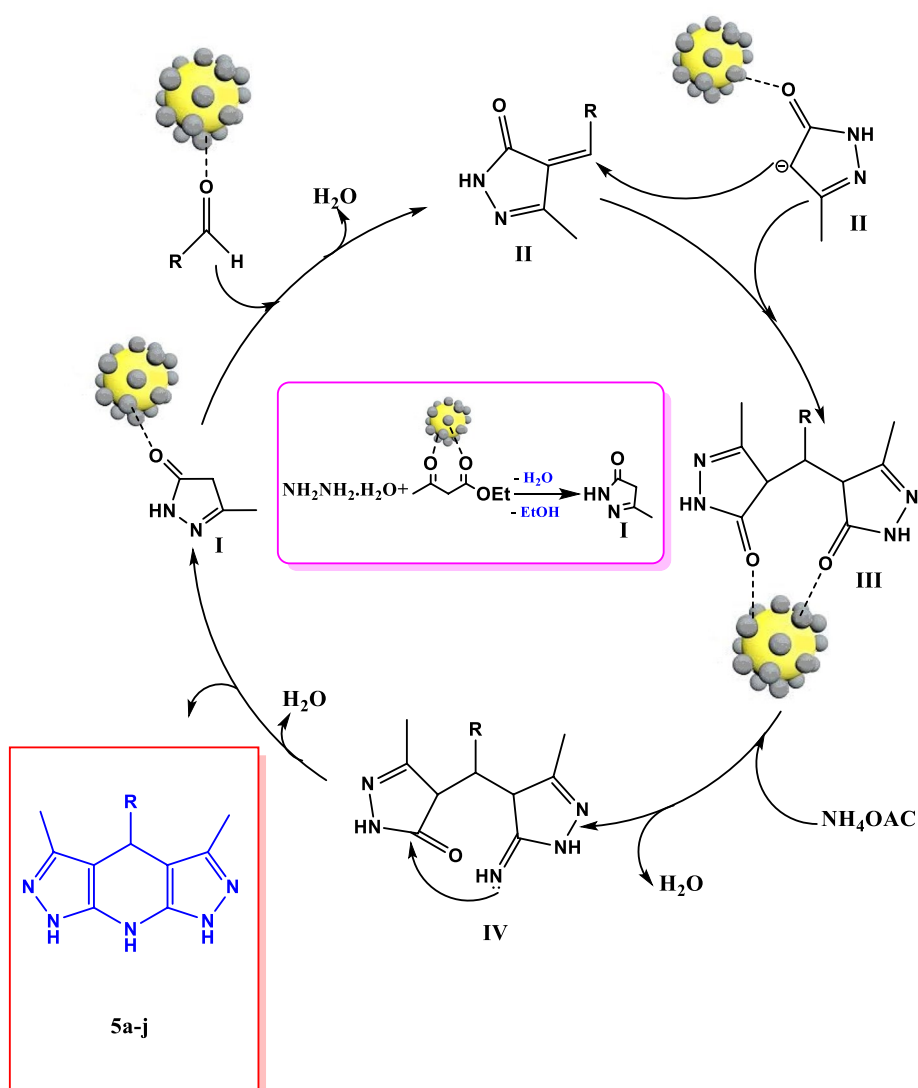
Figure 9. The suggested mechanism for the synthesis of 5a–j by using Fe_3O_4/Se.

bonyl groups subjected to the nucleophilic attack of hydrazine hydrate with two nucleophilic sites. In this step, a pyrazolone ring is formed (intermediate I) by removing water and ethanol molecules. Intermediate II was then created by the Knoevenagel condensation of activated aldehydes by the catalyst and pyrazolone ring. The reaction proceeds with the aid of Michael addition by assaulting the second ring of pyrazolone from intermediate (II) and intermediate (III). In the presence of an ammonium acetate catalyst, by attacking intermediate (III), compound IV was formed. In the final stage, compounds 5a-j were synthesized by removing water, performing intramolecular cyclization, and polymerizing compound IV[77,78]. Also, selenium can absorb carbonyl oxygen with its positive charge property.

Valuation of the efficiency of Fe_3O_4/Se nanocatalyst in the synthesis of pyrazolopyridine derivatives heterocyclic in contrast with other reported studies. A comparison of their catalytic performance was performed to evaluate the benefit of this catalyst over other previously reported catalysts in the synthesis of the 5 k derivative, and the results are shown in Table S1. The results show that the current technology is superior in terms of catalyst biocompatibility, use of an ecologically friendly solvent, and generation of the desired products with high yields in a reasonable amount of time under mild reaction conditions.

Reusability of Fe_3O_4/Se. In terms of industrial and commercial considerations, catalyst reusability is one of the most significant variables, and the ability to recycle products can largely lead the reaction process to conform to the concepts of green chemistry. The recoverability and reusability of the Fe_3O_4/Se nanocatalyst were assessed in the synthesis of 5b. Because of the magnetic nature of the catalyst, it can be easily isolated from the reaction mixture using a magnet bar, repeatedly rinsed with distilled water and ethanol, and then dried after each run. Fortunately, after six consecutive cycles, very little catalyst deactivation occurred during pyrazolopyridine synthesis (Fig. 10). The X-ray pattern of the recycled catalyst was almost identical to that of the fresh catalyst (Fig. S7).

Conclusion

In summary, new, efficient, low-cost, and reusable Fe_3O_4/Se NPs were produced and synthesized as nanocomposites using a simple coprecipitation technique. Various analytical methods have been used to evaluate nanocomposite structure, morphology, surface area, pore volume, pore size (width), magnetic properties, and antibacterial characteristics. The SEM images verified the stability and integrity of the spherical structure, as well as the excellent dispersion of Se NPs on the Fe_3O_4 surface. The magnetic properties of the nanocomposites were confirmed by VSM analysis. Additionally, detailed information, including the surface area, pore volume, and pore size (width) of the Fe_3O_4/Se catalytic system, was calculated using the (Brunauer–Emmett–Teller (BET)) and (Barrett–Joyner–Halenda (BJH)) methods. This shows that the synthesized nanocatalyst had a suitable surface area and pore size to promote organic reactions. The nanocomposite was employed as a well-organized and recyclable heterogeneous nanocatalyst for the production of pyrazolopyridine products via a four-component reaction. At room temperature and under mild reaction conditions, high to excellent product yields were achieved using Fe_3O_4/Se as a nanocatalyst. The catalyst can be simply removed from the reaction medium by an external magnetic field, washed and dried, and used several times without a substantial loss of activating sites. The antibacterial properties of this nanocomposite were investigated in the removal and destruction of G⁺ *S. aureus*, *S. saprophyticus*, G⁻ *E. coli*, *K. pneumonia*, *P. aeruginosa* bacteria, a group of dangerous bacteria that threaten the health of living organisms. This nanocomposite can also be utilized to disinfect water polluted with bacteria;
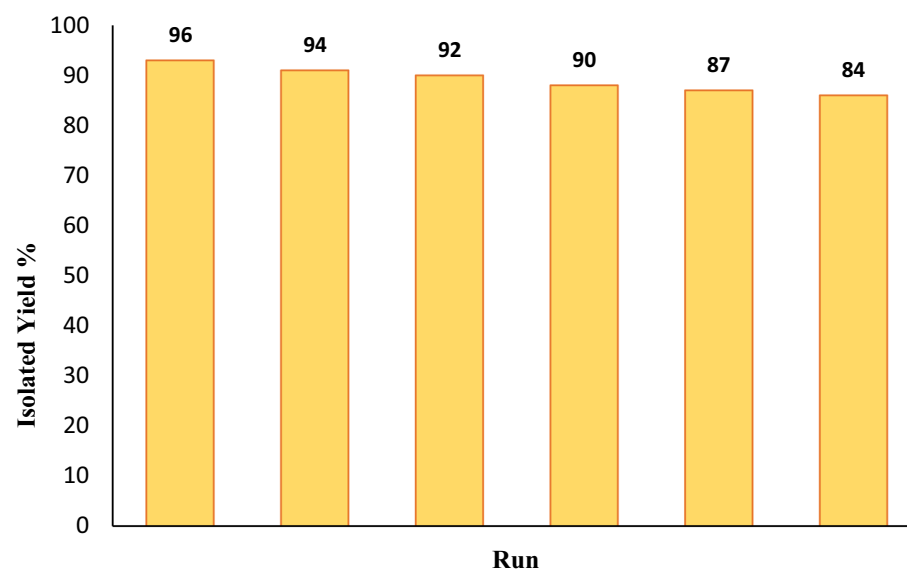
Figure 10. Recyclability of the Fe_3O_4/Se catalyst in the synthesis of **5b**.

the inactivation of *S. aureus* and *E. coli* in the presence of nanoparticles was confirmed by the colony method. Moreover, this is the first report on the plan, production, functionalization, and characterization of the current nanocomposite, as well as its presentation as a heterogeneous nanocatalyst in a significant organic process. Pyrazolopyridine is one of the most important heterocyclic compounds with many biological activities. In this paper, we report an effective and practical method for the synthesis of pyrazolopyridine and its derivatives.

Data availability

All data generated or analysed during this study are included in this published article [and its supplementary information files].

References

1. Sarkar, J., Dey, P., Saha, S. & Acharya, K. Mycosynthesis of selenium nanoparticles. *Micro Nano Lett.* **6**, 599–602 (2011).
2. Vahdati, M. & Moghadam, T. T. Synthesis and characterization of selenium nanoparticles-lysozyme nanohybrid system with synergistic antibacterial properties. *Sci. Rep.* **10**, 12627 (2020).
3. Nastulyavichus, A. *et al.* Antibacterial coatings of Se and Si nanoparticles. *Appl. Surf. Sci* **469**, 220–225 (2019).
4. Ahghari, M. R., Soltaninejad, V. & Maleki, A. Synthesis of nickel nanoparticles by a green and convenient method as a magnetic mirror with antibacterial activities. *Sci. Rep.* **10**, 1–10 (2020).
5. Medina Cruz, D., Mi, G. & Webster, T. J. Synthesis and characterization of biogenic selenium nanoparticles with antimicrobial properties made by *Staphylococcus aureus*, methicillin-resistant *Staphylococcus aureus* (MRSA), *Escherichia coli*, and *Pseudomonas aeruginosa*. *J. Biomed. Mater. Res. Part A* **106**, 1400–1412 (2018).
6. Liu, J., Wu, D., Zhu, N., Wu, Y. & Li, G. Antibacterial mechanisms and applications of metal-organic frameworks and their derived nanomaterials. *Trends Food Sci. Technol.* **109**, 413–434 (2021).
7. Yang, S. Z. *et al.* Recent progress in the optical detection of pathogenic bacteria based on noble metal nanoparticles. *Microchim. Acta* **188**(8), 1–23 (2021).
8. Levy, S. B. & Marshall, B. Antibacterial resistance worldwide: Causes, challenges and responses. *Nat. Med.* **10**, S122–S129 (2004).
9. Cohen, M. L. Changing patterns of infectious disease. *Nature* **406**, 762–767 (2000).
10. Singh, A., Dubey, S. & Dubey, H. K. Nanotechnology: The future engineering. *Nanotechnology* **6**, 230–233 (2019).
11. Eivazzadeh-Keihan, R. *et al.* Functionalized magnetic nanoparticles for the separation and purification of proteins and peptides. *TrAC Trends Anal. Chem.* **141**, 116291 (2021).
12. Amiri-Khamakani, Z., Hassanzadeh-Afruzi, F. & Maleki, A. Magnetized dextrin: Eco-friendly effective nanocatalyst for the synthesis of dihydropyrano [2, 3-c] pyrazole derivatives. *Chem. Proc.* **3**, 101 (2020).
13. Schwaminger, S. P. *et al.* Design of interactions between nanomaterials and proteins: A highly affine peptide tag to bare iron oxide nanoparticles for magnetic protein separation. *Biotechnol. J.* **14**, 1800055 (2019).
14. Kamalzare, M., Ahghari, M. R., Bayat, M. & Maleki, A. Fe$_3$O$_4$@ chitosan-tannic acid bionanocomposite as a novel nanocatalyst for the synthesis of pyranopyrazoles. *Sci. Rep.* **11**, 1–10 (2021).
15. Schwaminger, S. P. *et al.* Bio-nano interactions: Cellulase on iron oxide nanoparticle surfaces. *Adsorption* **23**, 281–292 (2017).
16. Morte, E. F. B. *et al.* Modified magnetite nanoparticle as biocatalytic support for magnetically stabilized fluidized bed reactors. *J. Mater. Res. Technol.* **14**, 1112–1125 (2021).
17. Lesiak, B. *et al.* Surface study of Fe$_3$O$_4$ nanoparticles functionalized with biocompatible adsorbed molecules. *Front. Chem.* **7**, 642 (2019).
18. Alam, H., Khatoon, N., Raza, M., Ghosh, P. C. & Sardar, M. Synthesis and characterization of nano selenium using plant biomolecules and their potential applications. *Bionanoscience* **9**, 96–104 (2019).
19. Toufektsian, M. C. *et al.* Effects of selenium deficiency on the response of cardiac tissue to ischemia and reperfusion. *Toxicology* **148**, 125–132 (2000).
20. Rayman, M. P. The importance of selenium to human health. *The Lancet* **356**, 233–241 (2000).
21. Manivasagan, P., Venkatesan, J., Sivakumar, K. & Kim, S. K. Pharmaceutically active secondary metabolites of marine actinobacteria. *Microbiol. Res.* **169**, 262–278 (2014).
22. Chuai, H. *et al.* Small molecule selenium-containing compounds: Recent development and therapeutic applications. *Eur. J. Med. Chem.* **223**, 113621 (2021).
23. Geoffrion, L. D. *et al.* Naked selenium nanoparticles for antibacterial and anticancer treatments. *ACS Omega* **5**, 2660–2669 (2020).
24. Alvi, G. B. *et al.* Biogenic selenium nanoparticles (SeNPs) from citrus fruit have anti-bacterial activities. *Sci. Rep.* **11**, 1–11 (2021).
25. Wang, C. Y., Makvandi, P., Zare, E. N., Tay, F. R. & Niu, L. N. Advances in antimicrobial organic and inorganic nanocompounds in biomedicine. *Adv. Ther.* **3**, 2000024 (2020).
26. Zhang, J. *et al.* Development, physicochemical characterization and cytotoxicity of selenium nanoparticles stabilized by beta-lactoglobulin. *Int. J. Biol. Macromol.* **107**, 1406–1413 (2018).
27. Jay, V. & Shafkat, R. Synthesis of selenium nanoparticles using Allium sativum extract and analysis of their antimicrobial property against gram positive bacteria. *Pharma Innov.* **7**, 262–266 (2018).
28. Zhang, Y. *et al.* Enhancement of cell permeabilization apoptosis-inducing activity of selenium nanoparticles by ATP surface decoration. Nanomedicine nanotechnology. *Biol. Med.* **9**, 74–84 (2013).
29. Ranjitha, V. R. & Rai, V. R. Selenium nanostructure: Progress towards green synthesis and functionalization for biomedicine. *Int. J. Pharm Investig.* **51**, 117–135 (2021).
30. Amani, H. *et al.* Selenium nanoparticles for targeted stroke therapy through modulation of inflammatory and metabolic signaling. *Sci. Rep.* **9**, 1–15 (2019).
31. Prasad, K. S., Patel, H., Patel, T., Patel, K. & Selvaraj, K. Biosynthesis of Se nanoparticles and its effect on UV-induced DNA damage. *Colloids Surf. B Biointerfaces* **103**, 261–266 (2013).
32. Shen, Q. *et al.* Antioxidant activity in vitro of the selenium-contained protein from the Se-enriched Bifidobacterium animalis 01. *Anaerobe* **16**, 380–386 (2010).
33. Valko, M., Rhodes, C. J. B., Moncol, J., Izakovic, M. M. & Mazur, M. Free radicals, metals and antioxidants in oxidative stress-induced cancer. *Chem. Biol. Interact.* **160**, 1–40 (2006).
34. Yu, B., Zhang, Y., Zheng, W., Fan, C. & Chen, T. Positive surface charge enhances selective cellular uptake and anticancer efficacy of selenium nanoparticles. *Inorg. Chem.* **51**, 8956–8963 (2012).
35. Manjare, S. T., Kim, Y. & Churchill, D. G. Selenium-and tellurium-containing fluorescent molecular probes for the detection of biologically important analytes. *Acc. Chem. Res.* **47**, 2985–2998 (2014).
36. Wang, L., Hu, C. & Shao, L. The antimicrobial activity of nanoparticles: Present situation and prospects for the future. *Int. J. Nanomed.* **12**, 1227 (2017).

37. He, J. *et al.* High speed water purification and efficient phosphate rejection by active nanofibrous membrane for microbial contamination and regrowth control. *Chem. Eng. J.* **337**, 428–435 (2018).

38. Husband, P. S. & Boxall, J. B. Asset deterioration and discolouration in water distribution systems. *Water Res.* **45**, 113–124 (2011).

39. Betanzo, E. W., Hofmann, R., Hu, Z., Baribeau, H. & Alam, Z. Modeling the impact of microbial intrusion on secondary disinfection in a drinking water distribution system. *J. Environ. Eng.* **134**, 231–237 (2008).

40. Thayanukul, P., Kurisu, F., Kasuga, I. & Furumai, H. Evaluation of microbial regrowth potential by assimilable organic carbon in various reclaimed water and distribution systems. *Water Res.* **47**, 225–232 (2013).

41. Shaw, J. L. A. *et al.* Assessing the impact of water treatment on bacterial biofilms in drinking water distribution systems using high-throughput DNA sequencing. *Chemosphere* **117**, 185–192 (2014).

42. Figueras, M. J. & Borrego, J. J. New perspectives in monitoring drinking water microbial quality. *Int. J. Environ. Res. Public Health* **7**, 4179–4202 (2010).

43. Kumar, S., Anwer, R., Sehrawat, A., Yadav, M. & Sehrawat, N. Assessment of bacterial pathogens in drinking water: A serious safety concern. *Curr. Pharmacol. Rep.* **7**, 206–212 (2021).

44. Zhu, T. *et al.* Comparison of performance of two large-scale vertical-flow constructed wetlands treating wastewater treatment plant tail-water: Contaminants removal and associated microbial community. *J. Environ. Manage.* **278**, 111564 (2021).

45. Bhateria, R. & Jain, D. Water quality assessment of lake water: A review. *Sustain. Water Resour. Manag.* **2**, 161–173 (2016).

46. Fong, T. T. & Lipp, E. K. Enteric viruses of humans and animals in aquatic environments: Health risks, detection, and potential water quality assessment tools. *Microbiol. Mol. Biol. Rev.* **69**, 357–371 (2005).

47. Pang, Z., Raudonis, R., Glick, B. R., Lin, T.-J. & Cheng, Z. Antibiotic resistance in *Pseudomonas aeruginosa*: Mechanisms and alternative therapeutic strategies. *Biotechnol. Adv.* **37**, 177–192 (2019).

48. Ahghari, M. A., Ahghari, M. R., Kamalzare, M. & Maleki, A. Design, synthesis, and characterization of novel eco-friendly chitosan-AgIO$_3$ bionanocomposite and study its antibacterial activity. *Sci. Rep.* **12**, 1–13 (2022).

49. Zare-Bakheir, E., Ahghari, M. R., Maleki, A. & Ghafuri, H. Synthesis of Cu (OH) 2 nanowires modified by Fe$_3$O$_4$@ SiO$_2$ nanocomposite via green and innovative method with antibacterial activity and investigation of magnetic behaviours. *R Soc. Open Sci.* **9**, 212025 (2022).

50. Masoud, W. *et al.* The fate of indigenous microbiota, starter cultures, *Escherichia coli*, *Listeria innocua* and *Staphylococcus aureus* in Danish raw milk and cheeses determined by pyrosequencing and quantitative real time (qRT)-PCR. *Int. J. Food Microbiol.* **153**, 192–202 (2012).

51. Bakhshandeh, B. *et al.* New analytical methods using carbon-based nanomaterials for detection of Salmonella species as a major food poisoning organism in water and soil resources. *Chemosphere* **287**, 132243 (2022).

52. Hadinoto, K. & Cheow, W. S. Nano-antibiotics in chronic lung infection therapy against *Pseudomonas aeruginosa*. *Colloids Surf. B Biointerfaces* **116**, 772–785 (2014).

53. Rada, B. Interactions between neutrophils and *Pseudomonas aeruginosa* in cystic fibrosis. *Pathogens* **6**, 10 (2017).

54. Pang, Z., Raudonis, R., Glick, B. R., Lin, T. J. & Cheng, Z. Antibiotic resistance in *Pseudomonas aeruginosa*: Mechanisms and alternative therapeutic strategies. *Biotechnol. Adv.* **37**, 177–192 (2019).

55. Hameed, A. S. H. *et al.* In vitro antibacterial activity of ZnO and Nd doped ZnO nanoparticles against ESBL producing *Escherichia coli* and *Klebsiella pneumoniae*. *Sci. Rep.* **6**, 1–11 (2016).

56. Valenzuela-Valderrama, M., González, I. A. & Palavecino, C. E. Photodynamic treatment for multidrug-resistant Gram-negative bacteria: Perspectives for the treatment of *Klebsiella pneumoniae* infections. *Photodiagnosis Photodyn. Ther.* **28**, 256–264 (2019).

57. Cowan, S. W. *et al.* Crystal structures explain functional properties of two *E. coli* porins. *Nature* **358**, 727–733 (1992).

58. Archer, N. K. *et al.* *Staphylococcus aureus* biofilms: Properties, regulation, and roles in human disease. *Virulence* **2**, 445–459 (2011).

59. Zhang, H. *et al.* Antibacterial properties and mechanism of selenium nanoparticles synthesized by Providencia sp. DCX. *Environ. Res.* **194**, 110630 (2021).

60. Shabalala, N. G., Pagadala, R. & Jonnalagadda, S. B. Ultrasonic-accelerated rapid protocol for the improved synthesis of pyrazoles. *Ultrason. Sonochem.* **27**, 423–429 (2015).

61. García, M., Romero, I. & Portilla, J. Synthesis of fluorescent 1, 7-dipyridyl-bis-pyrazolo [3, 4-b: 4′, 3′-e] pyridines: Design of reversible chemosensors for nanomolar detection of Cu^{2+}. *ACS Omega* **4**, 6757–6768 (2019).

62. Maleki, A., Hajizadeh, Z. & Salehi, P. Mesoporous halloysite nanotubes modified by CuFe$_2$O$_4$ spinel ferrite nanoparticles and study of its application as a novel and efficient heterogeneous catalyst in the synthesis of pyrazolopyridine derivatives. *Sci. Rep.* **9**, 5552 (2019).

63. El-Gohary, N. S. & Shaaban, M. I. New pyrazolopyridine analogs: Synthesis, antimicrobial, antiquorum-sensing and antitumor screening. *Eur. J. Med. Chem.* **152**, 126–136 (2018).

64. Anand, D. *et al.* Antileishmanial activity of pyrazolopyridine derivatives and their potential as an adjunct therapy with miltefosine. *J. Med. Chem.* **60**, 1041–1059 (2017).

65. Wenglowsky, S. *et al.* Pyrazolopyridine inhibitors of B-RafV600E. Part 1: The development of selective, orally bioavailable, and efficacious inhibitors. *ACS Med. Chem. Lett.* **2**, 342–347 (2011).

66. Liu, Y., Liu, P., Su, Z., Li, F. & Wen, F. Attapulgite–Fe$_3$O$_4$ magnetic nanoparticles via co-precipitation technique. *Appl. Surf. Sci.* **255**, 2020–2025 (2008).

67. Tabaraki, R. & Sadeghinejad, N. Comparison of magnetic Fe$_3$O$_4$/chitosan and arginine-modified magnetic Fe$_3$O$_4$/chitosan nanoparticles in simultaneous multidye removal: Experimental design and multicomponent analysis. *Int. J. Biol. Macromol.* **120**, 2313–2323 (2018).

68. Chen, J. *et al.* Construction of selenium-embedded mesoporous silica with improved antibacterial activity. *Colloids Surf. B Biointerfaces* **190**, 110910 (2020).

69. Huang, T., Holden, J. A., Heath, D. E., O'Brien-Simpson, N. M. & O'Connor, A. J. Engineering highly effective antimicrobial selenium nanoparticles through control of particle size. *Nanoscale* **11**, 14937–14951 (2019).

70. Dabiri, M., Salehi, P., Kooshkari, M., Hajizadeh, Z. & MaGee, D. I. An efficient synthesis of tetrahydropyrazolopyridine derivatives by a one-pot tandem multi-component reaction in a green media. *ARKIVOC* **4**, 204–214 (2014).

71. Zhao, K., Lei, M., Ma, L. & Hu, L. A facile protocol for the synthesis of 4-aryl-1, 4, 7, 8-tetrahydro-3, 5-dimethyldipyrazolo [3, 4-b: 4′, 3′-e] pyridine derivatives by a Hantzsch-type reaction. *Monatshefte Che.-Chem. Mon.* **142**, 1169–1173 (2011).

72. Shabalala, N. G., Pagadala, R. & Jonnalagadda, S. B. Ultrasonic-accelerated rapid protocol for the improved synthesis of pyrazoles. *Ultrason. Sonochem.* **27**, 423–429 (2015).

73. Shahbazi-Alavi, H. *et al.* Nano-CuCr$_2$O$_4$: An efficient catalyst for a one-pot synthesis of tetrahydrodipyrazolopyridine. *J. Chem. Res.* **40**, 361–363 (2016).

74. Sadeghzadeh, S. M. A heteropolyacid-based ionic liquid immobilized onto magnetic fibrous nano-silica as robust and recyclable heterogeneous catalysts for the synthesis of tetrahydrodipyrazolopyridines in water. *RSC Adv.* **6**, 75973–75980 (2016).

75. Safaei-Ghomi, J., Sadeghzadeh, R. & Shahbazi-Alavi, H. A pseudo six-component process for the synthesis of tetrahydrodipyrazolo pyridines using an ionic liquid immobilized on a FeNi$_3$ nanocatalyst. *RSC Adv.* **6**, 33676–33685 (2016).

76. Sadeghzadeh, S. M. A heteropolyacid-based ionic liquid immobilized onto magnetic fibrous nano-silica as robust and recyclable heterogeneous catalysts for the synthesis of tetrahydrodipyrazolopyridines in water. *RSC Adv.* **6**, 75973–75980 (2016).

77. Shao, L., Li, Y., Lu, J. & Jiang, X. Recent progress in selenium-catalyzed organic reactions. *Org. Chem. Front.* **6**, 2999–3041 (2019).

78. Freudendahl, D. M., Santoro, S., Shahzad, S. A., Santi, C. & Wirth, T. Green chemistry with selenium reagents: Development of efficient catalytic reactions. *Angew. Chem. Int. Ed.* **48**, 8409–8411 (2009).

Acknowledgements

Author contributions

M.R.A. carried out the analyses and characterization and participated in discussing the results. Z.A. prepared the draft of the manuscript and revised the manuscript. A.M. has designed the study and managed the project. All authors read and approved the final manuscript.

Competing interests

The authors declare no competing interests.

Additional information

Supplementary Information The online version contains supplementary material available at https://doi.org/10.1038/s41598-023-28284-x.

Correspondence and requests for materials should be addressed to A.M.

Reprints and permissions information is available at www.nature.com/reprints.

Publisher's note Springer Nature remains neutral with regard to jurisdictional claims in published maps and institutional affiliations.